Results in Physics 67 (2024) 108035

Contents lists available at ScienceDirect

Results in Physics

journal homepage: www.elsevier.com/locate/rinp

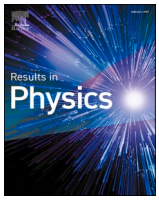

Towards the CdS/SnSe solar cell optimization: Understanding the transport mechanisms

A. Carrillo-Osuna [a], F.J. Sánchez-Rodríguez [a], K.G. Rodriguez-Osorio [b], I. Montoya De Los Santos [c], J.P. Morán-Lázaro [b], M. Ojeda-Martínez [b], Laura M. Pérez [d,*], David Laroze [e], Maykel Courel [b,*]

[a] Facultad de Ciencias Físico-Matemáticas, Universidad Autónoma de Sinaloa, C.P. 80010, Culiacán, Sinaloa, México
[b] Centro Universitario de los Valles, Universidad de Guadalajara, Carretera Guadalajara—Ameca Km. 45.5, Ameca C.P. 46600, Jalisco, Mexico
[c] Instituto de Estudios de La Energía, Universidad del Istmo, 70760 Santo Domingo Tehuantepec, Oaxaca, Mexico
[d] Departamento de Ingeniería Industrial y de Sistemas, Universidad de Tarapacá, Casilla 7 D, Arica 1000000, Chile
[e] Instituto de Alta Investigación, Universidad de Tarapacá, Casilla 7 D, Arica 1000000, Chile

ARTICLE INFO

Keywords:
SnSe solar cell
Modeling and simulation
Loss transport mechanisms
Device optimization

ABSTRACT

In this work, numerical simulation results on SnSe solar cells are presented. The influence of loss mechanisms such as radiative recombination, SnSe bulk recombination, and CdS/SnSe interface recombination on the device is studied in detail under and without the influence of resistances for the first time. In the first step, our model is validated by accurately reproducing the experimental available data. We found that non-radiative recombination originated by SnSe bulk defects in combination with high series resistances are dominant loss mechanisms, resulting in efficiency values lower than 2 %. In addition, the important role of the CdS/SnSe interface is also evidenced, since SnSe solar cells without bulk defects and resistances would not be able to overcome the efficiency barrier of 10 % because of the cliff-like band alignment. The role of each loss mechanism on SnSe solar cell performance was studied as a function of material thicknesses, carrier concentrations, bulk and interface defects, and resistances for device optimization. We demonstrated that conversion efficiency of 21.8 % with an open-circuit voltage, short-circuit current density, and fill factor values of 0.82 V, 31.6 mA/cm^2, 84.6 %, respectively can be achieved in the optimized device under the standard conditions of AM 1.5G illumination and 300 K.

Introduction

Currently, single-junction photovoltaics based on CIGS, and CdTe have shown the highest photoconversion efficiencies (PCE) with values higher than 20 % under AM 1.5 solar spectrum at 25 °C [1]. However, the use of these semiconductors has several economic and environmental concerns. First, some of the main constituent elements are non-abundant, for example, elements such as Te, In, and Ga are prone to limit this technology since the annual production rates are around 135, 167, and 600 tons, respectively in comparison to other elements such as Se and Sn, whose lowest annual production rate is 2,200 tons for Se and the greatest is 280,000 tons for Sn [2,3]. Second, it is well known that Cd and Te are potentially harmful to the environment and human health. The increasing demand for energy along with the necessity of developing energy sources that are clean, sustainable, and scalable have motivated the scientific community to research alternative non-toxic, abundant, and affordable novel materials to try to achieve higher efficiencies. In the last decade, tin selenide (SnSe) has received a great deal of attention because of its optoelectronic properties, which make it an adequate candidate for photovoltaics. SnSe, a binary VI-VI material, exhibits an orthorhombic crystal structure and typically *p*-type conductivity owing to Sn-vacancies [4]. Furthermore, it has been described by an optical band gap (Eg) ranging from 0.95 to 1.3 eV, which is near the optimal one for solar cell application. In addition, a high absorption coefficient of around 10^5 cm^{-1} has been reported for SnSe material due to the direct band gap transitions, which guarantees the highest photon absorption at lower thicknesses. Besides, tin and selenium, are abundant elements in the Earth's crust, so the reactants used for synthesizing SnSe thin films are affordable and additionally exhibit low toxicity [5–7]. In addition, the simplicity of using only two elements makes the formation of secondary phases less likely during thin film deposition, unlike other complex compounds like the kesterite family consisting of four or more

* Corresponding authors.
E-mail addresses: lperez@academicos.uta.cl (L.M. Pérez), maykel.courel@academicos.udg.mx (M. Courel).

https://doi.org/10.1016/j.rinp.2024.108035
Received 15 August 2024; Received in revised form 20 October 2024; Accepted 4 November 2024
Available online 6 November 2024

elements [8]. Some works have been focused on showing the viability of photovoltaic devices based on SnSe material. In 2012, *Mathews et al* first fabricated a SnSe/CdS solar cell through electrodeposition, which exhibited a conversion efficiency of 0.03 %. Although this device showed very poor efficiency, it demonstrated that photovoltaic applications of SnSe are possible [9]. Nowadays, SnSe-based solar cells have been developed with efficiencies from 0.1 % to 6.44 % employing different approaches [10–13]. Despite the effort exerted on improving the PCE of SnSe-based photovoltaics, its maximum efficiencies are far from being the theoretically predicted efficiency. The Shockley-Queisser (SQ) report establishes the highest possible photovoltaic characteristics for single-junction devices. For tin selenide (Eg ~ 1.2 eV), the efficiency given by the SQ limit is roughly 33 %, while for the rest of the characteristics, namely, short-circuit current density (J_{sc}), fill factor (FF), and open-circuit voltage (V_{oc}) are 39.99 mA/cm^2, 87.7 %, and 0.94 mV, respectively [14]. Recent studies using SCAPS-1D simulation have shown that SnSe-based thin film solar cells under optimized conditions can achieve efficiencies close to the SQ limit. *Yadav et al* performed a simulation study based on an experimental report in which they optimized and compared two *Mo/SnSe/CdS/i-ZnO/AZO/Al* solar cells, with and without a NiO back-surface field layer. The highest efficiency achieved was 2.69 % and they concluded that the presence of the BSF layer improved V_{oc} and FF [15]. Similarly, *Kumar et al* simulated a *Mo/SnSe/CdS/i-ZnO/ITO/Mo* solar cell varying thickness, band gap, density of states, radiative recombination coefficient (RRC), and acceptor concentration (N_A) in SnSe, achieving an efficiency of 27.72 % [16]. However, in these two works several remarks can be made about the use of *i*-ZnO, very thin CdS layers, and how to tune some of the parameters varied such as the radiative recombination coefficient (RRC), or electron-to-hole mobility ratios (μ_n:μ_p). On the other hand, there are no available theoretical and experimental studies on device behavior considering the influence of likely loss mechanisms, which could help to enhance device efficiency. Traditional deposition techniques for SnSe thin films entail the formation of bulk defects, which play a dominant role in carrier transport. In addition, since CdS and SnSe are described by different lattice parameters and crystalline structures, the formation of interface defects is expected, which can degrade the device's performance. However, a comprehensive study on the impact of radiative recombination and non-radiative recombination based on bulk and interface defects on CdS/SnSe solar cells is still pending. A detailed study on the role of bulk and interface defects along with resistances in SnSe solar cells can provide information on conditions required at the laboratory level to achieve a new efficiency record. Based on the current state-of-the-art literature, this work presents a deep understanding of the influence of radiative, bulk, and interface recombination on CdS/SnSe solar cells for the first time. An in-depth analysis of the behavior of the different loss mechanisms as a function of absorber and buffer thicknesses, SnSe acceptor concentration, CdS donor concentration, and defect densities is presented. Furthermore, the role of series and shunt resistances on SnSe solar cells is also evaluated. For this purpose, a typical single-junction ITO/CdS/SnSe/Au device is simulated and optimized using SCAPS-1D to establish a set of parameters to consider for further experimental development. Our model is validated by reproducing the experimental information reported for a CdS/SnSe solar cell with an efficiency of 0.63 % [10]. After the model validation, we demonstrated that efficiencies slightly above 20 % can be achieved without the inclusion of BSF, only by varying parameters that are easily tuned experimentally. The parameters considered for the optimization are the buffer and absorber thickness, the buffer/absorber interface and SnSe defect densities, the absorber acceptor density and buffer donor density, and device resistances. In this sense, this work provides the experimental groups with not only the knowledge of the main causes of low CdS/SnSe solar cell performances but also introduces the path guide to be implemented at laboratories to further efficiency promotion.

This paper is organized as follows: Section 2 presents the model details focusing on the main semiconductor equations to perform the numerical simulations, with a particular emphasis on the most likely loss mechanisms governing SnSe solar cells. In Section 3, in the first step, the numerical validation of the model is presented by comparing the model outcomes with the experimental data. After that, the influence of buffer and absorber thicknesses and carrier concentrations, as well as SnSe bulk and SnSe/CdS interface defects on solar cell performance is evaluated under and without the effect of resistances to find material properties that result in the device optimization. Finally, the conclusions of the work are presented in Section 4.

Solar cell structure and model details

The CdS/SnSe solar cell has the Au/SnSe/CdS/ITO structure, where ITO, CdS, and SnSe are the transparent conducting oxide, buffer, and absorber layers, respectively and Au is the metallic contact (MC). The solar cell is thus composed of three semiconducting layers and a metallic contact as shown in Fig. 1. For the simulation of the Au/SnSe/CdS/ITO solar cell, the software SCAPS-1D is used. SCAPS finds the numerical solution under steady-state conditions to transport equations by using the Newton–Raphson method through the Gummel iterative scheme [17], providing the photovoltaic characteristics. The semiconductor equations in one dimension are the Poisson equation:

$$\frac{\partial}{\partial x}\left(\epsilon\epsilon_0\frac{\partial \Psi}{\partial x}\right) = -q\left(p - n + N_D - N_A + \frac{\rho_{def}}{q}\right) \tag{1}$$

In this equation, ψ is the electric potential across the *p-n* junction, N_A is the acceptor concentration, N_D is the donor concentration, p and n are the hole and electron concentrations, respectively, q is the elementary charge, and $\epsilon\epsilon_0$ is the semiconductor permittivity. Finally, ρ_{def} is the charge density due to defects. The drift current equations for electrons and holes:

$$\begin{cases} J_n = -qp\mu_n\left(\dfrac{\partial E_{Fn}}{\partial x}\right) \\ J_p = qn\mu_p\left(\dfrac{\partial E_{Fp}}{\partial x}\right) \end{cases} \tag{2}$$

Where, μ is the charge carrier mobility, E_{Fp} and E_{Fn} stand for the quasi-Fermi levels splatted under illumination. Finally, the carrier continuity equations:

$$\begin{cases} \dfrac{1}{q}\dfrac{\partial J_n}{\partial x} + G(x) - R_n(n,p) = 0 \\ \dfrac{1}{q}\dfrac{\partial J_p}{\partial x} - G(x) + R_p(n,p) = 0 \end{cases} \tag{3}$$

Where, $G(x)$ and $R(n,p)$ are electron–hole generation and recombination rates, respectively. To perform calculations, SCAPS requires the user to input the electrical and optical properties of each layer of the device. The simulation was conducted at 300 K and AM 1.5G spectrum (1000 W/m^2), and the optoelectronic and geometric properties of the layers are summarized in Table 1. The initial layer thicknesses used for simulations are mainly based on the light penetration depth. For optical calculations, uniform optical absorption coefficients were assumed. In addition, default CdS and ITO absorption coefficient dependence on wavelength given by SCAPS were used. SnSe absorption coefficient as a function of wavelength was calculated from the semiconductor theory

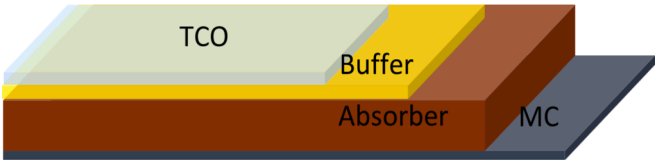

Fig. 1. Structure of the p-n heterojunction solar cell based on CdS/SnSe.

Table 1
Geometric and optoelectronic properties of the semiconductor layers that build up the CdS/SnSe solar cell.

Parameters	Layer		
	SnSe	CdS	ITO
Thickness, t (nm)	800	100	400
Band gap, E_g (eV)	1.2	2.45	3.65
Electron affinity, χ (eV)	4.1 [18]	4.4	4.8
Dielectric permittivity, ε (relative)	9.94 [19]	10	8.9
Conduction band density of states ($1/cm^3$)	1.96×10^{19}	2.2×10^{18}	5.2×10^{18}
Valence band density of states ($1/cm^3$)	3.8×10^{18}	1.8×10^{19}	1.0×10^{18}
Electron thermal velocity (cm/s)	7.3×10^{6}	1×10^{7}	1×10^{7}
Hole thermal velocity (cm/s)	1.25×10^{7}	1×10^{7}	1×10^{7}
Electron mobility, μ_n (cm^2/Vs)	125	100	10
Hole mobility, μ_p (cm^2/Vs)	371 [20]	50	10
Shallow donor density, N_D ($1/cm^3$)	0	1×10^{17}	1×10^{17}
Shallow acceptor density, N_A ($1/cm^3$)	1×10^{17}	0	0

concerning direct band gap transitions, where the absorption coefficient is proportional to $\sqrt{E-Eg}$, being E the photon energy, and Eg the absorber band gap. We assumed that light penetrates the ITO layer and transmits from ITO to the absorber, being attenuated in each layer by the familiar exponential function depending on the material band gap (Beer's law) as follows: $exp(-\alpha x)$. Furthermore, for calculations, reflection at the front surface and internal reflections were not required to reproduce the experimental data, which accounts for dominant losses owing to intrinsic defects rather than photon reflection. The SnS and CdS absorption coefficients as functions of wavelength used for calculations are presented in Fig. 2. Absorption coefficient values in the range of 10^4–10^5 cm^{-1} are representative of SnSe material, which accounts for a penetration depth of light lower than 1 μm. In this sense, SnSe thickness near 1 μm can be chosen to guarantee complete photon absorption.

The solar cell band diagram is shown in Fig. 3. In this band diagram, the rear surface of the absorber layer is at 0.0 μm, and the front surface of the windows layer is at 1.3 μm. The three different regions of the solar cell appear in this diagram, the narrower band gap region corresponds to the absorber, and it is seen that the successive layers have wider band gaps, which ease the transport of electrons but limit the transport of holes, then favoring the charge accumulation in the different regions but also recombination in the bulk or interface [21]. This behavior is common in heterojunction solar cells that show the type II band alignment, which has a negative conduction band offset, $\Delta E_c < 0$ [22]. A typical cliff-like alignment at the CdS/SnSe interface is observed in Fig. 3. Band

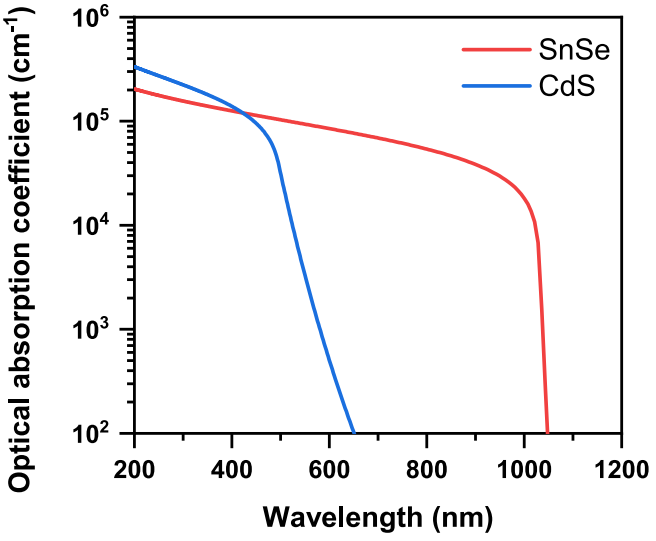

Fig. 2. Absorption coefficient dependence on wavelength for SnSe and CdS materials.

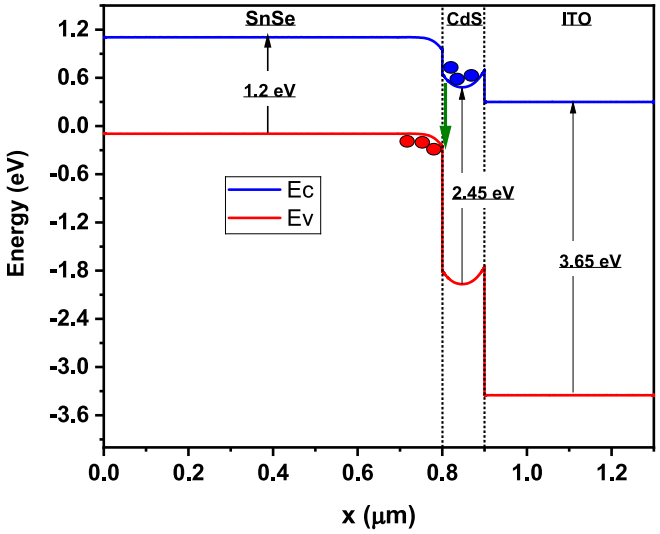

Fig. 3. Band diagram of CdS/SnSe solar cell.

offset values of 0.3 and 1.55 eV for conduction and valence bands, respectively are characteristics of CdS/SnSe solar cells, resulting in an effective band gap of 0.9 eV at the CdS/SnSe interface. This reduced band gap of 0.9 eV with respect to the SnSe one (1.2 eV) favors carrier recombination at the junction interface. When electron-hole pairs are created by the incident of light in SnSe and CdS materials, they diffuse until reaching the depletion zone where they are separated by the electric field of the junction, resulting in the electron drift to the CdS and holes to the SnSe material; in their transport near the heterointerface, they can recombine through interface defects due to the reduced band gap, typical of cliff-like heterojunction, as shown in Fig. 3. Losses at the CdS/SnSe interface are also justified by the fact that electrons are accumulated at the absorber/CdS interface, since they have to overcome a potential barrier of 210 meV to be transported to the ITO material, due to band bending because of the built-in voltage of the junction, while holes are not able to overcome a barrier of 1.55 eV due to the valence band offset, also accumulating near the CdS/SnSe interface. Therefore, in addition to recombination due to SnSe bulk defects, it is important to consider the role of interface defects in carrier transport, which is an important point analyzed in this work.

Sources of recombination

In this work, the most important sources of recombination are considered. The recombination mechanisms are radiative (band-to-band transitions), Shockley-Read-Hall (SRH), and non-radiative interface recombination due to buffer/absorber interface defects. Radiative band-to-band recombination stands for the lowest limit among the loss mechanisms, which rate can be calculated by:

$$U_{rad} = \kappa(np - n_i^2) \tag{4}$$

Where p, n, and n_i are the hole, electron, and intrinsic concentrations, respectively, and κ is the RRC, found by the detailed balance theory for semiconductors in thermal equilibrium, resulting in approximately 10^{-12} $cm^{-3}s^{-1}$

To analyze the impact of non-radiative recombination (SRH), two types of bulk defects at a single energy level are being considered. For the absorber and buffer layers, middle band gap defects are assumed to overestimate the impact of defects. The density of defects, N_t, in each semiconductor is treated as a variable, and therefore the carrier lifetime and diffusion length too [23,24]. The Shockley-Read-Hall recombination rate for a single-level trap is given by:

$$U_{SRH} = \frac{np - n_i^2}{\tau_n\left(p + n_i e^{\frac{E_t - E_i}{kT}}\right) + \tau_p\left(n + n_i e^{\frac{E_i - E_t}{kT}}\right)} \quad (5)$$

Where E_i is the intrinsic energy level and E_t is the trap energy in the semiconductor.

Similarly, the buffer/absorber interface recombination (IR) is described by Pauwels-Vanhoutte as a particular case of SRH recombination [25]. The defects in the interface were considered neutral and with a single energy level of 0.6 eV above the E_v of the absorber. The recombination rate for this mechanism can be evaluated by:

$$U_{IR} = S[p(0^+) - p_i] \quad (6)$$

Where S is the buffer/absorber interface recombination velocity, p is the hole concentration at the interface, $x = 0^+$, and p_i is the intrinsic hole concentration at the interface [22].

Results and discussion

Numerical validation of the model

For the numerical validation of the model, the results of a previously reported CdS/SnSe solar cell were used [10]. To replicate the J-V characteristics, parameters of the material and the device that were not detailed by the report are adjusted. As a first approach, the characteristics given in Table 1 were inputted into the software. Also, reported values of series and shunt resistances were used [6]. These values of R_s and R_{sh} are 54 Ωcm^2 and 106 Ωcm^2, respectively. Finally, we introduced bulk defects in SnSe, CdS, and CdS/SnSe interface defects. Fig. 4 shows the experimental and modeled J-V curves. In this first approach, the model does not match the experimental result. Hence, to fit the experimental data, bulk and interface defect properties were modified along with resistance values. In SnSe material, the density of defects was increased to 10^{20} cm^{-3} and the capture cross-section of holes and electrons was kept at 10^{-15} cm^2. In CdS, the density of defects was fixed at 8 x 10^{17} cm^{-3} with a hole and electron capture cross-section of 10^{-12} cm^2. The comparison between the experimental and theoretical data is shown in Fig. 5, the V_{oc} and J_{sc} values of the model are very close to the experimentally obtained ones. The fill factor value in Fig. 5 is mainly corrected by series and shunt resistance which were changed to 26.8 Ωcm^2 and 103 Ωcm^2, respectively. These resistance values will be considered as the representative ones in the next calculations.

In the original report on CdS/SnSe photovoltaics used to numerically validate the model, the external quantum efficiency (EQE) curve was not provided. Consequently, the EQE of the final model was obtained using the software. Fig. 6 shows the EQE of the CdS/SnSe solar cell adjusted model, which exhibits a maximum collection of charge carriers of 26 % at wavelengths around 540 nm. In addition, the solar cell is responding to the incoming light from 300 nm to around 1050 nm. A similar behavior of the EQE was reported for a CdS/SnSe solar cell with a different structure, indicating that in both solar cells, the active region is the same [15]. In this case, the low EQE shows the presence of different current density losses mainly attributed to recombination, which prevents the solar cell from achieving high efficiency.

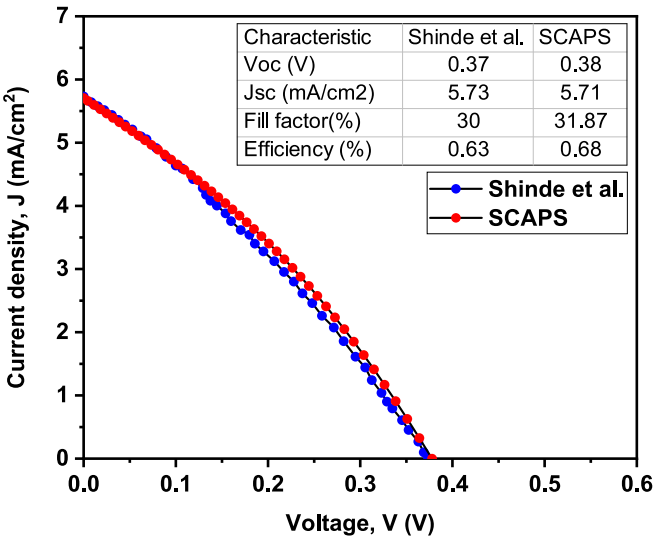

Fig. 5. J-V characteristics of the final adjusted CdS/SnSe solar cell model.

Effect of loss mechanisms on SnSe solar cell

To evaluate the effect of loss mechanisms, the current density–voltage characteristics under radiative recombination (R), Shockley-Read-Hall recombination (SRH) due to bulk defects, interface recombination (IR), and all mechanisms acting simultaneously were obtained. The J-V curves for the diverse recombination configurations under representative resistances are shown in Fig. 7(a). For all calculations, the radiative losses are assumed as default. The optoelectronic parameters of simulated devices are given in Table 2. The best J-V characteristics are

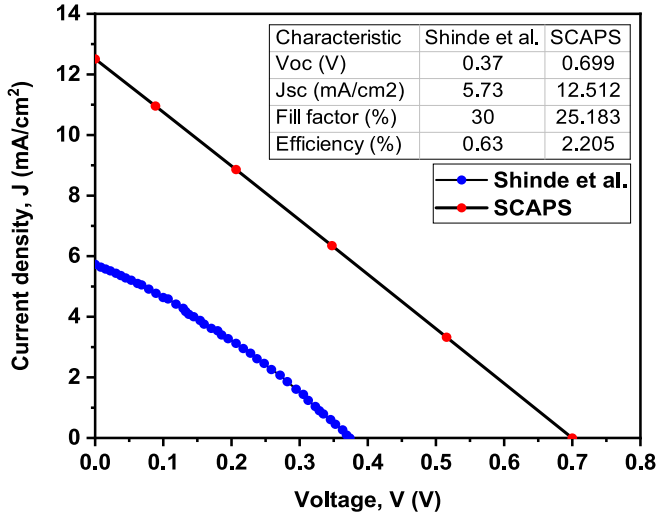

Fig. 4. J-V Characteristics of the first approach to the CdS/SnSe solar cell model.

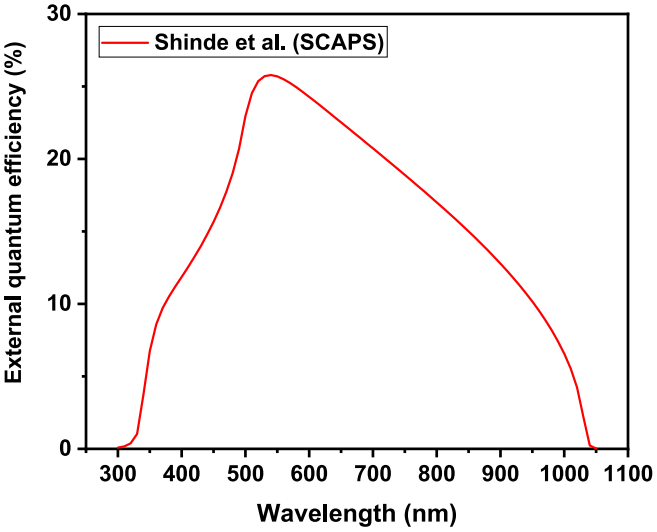

Fig. 6. External quantum efficiency of the CdS/SnSe solar cell adjusted model.

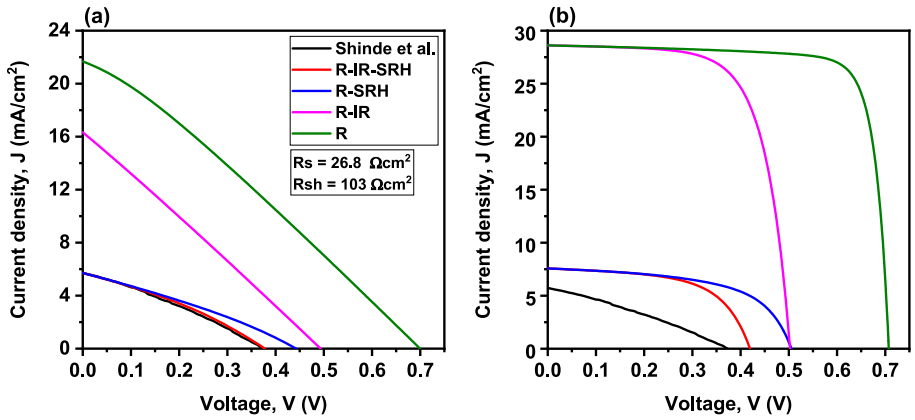

Fig. 7. J-V curves for different recombination mechanisms, (a) under representative resistances and (b) under ideal resistances.

Table 2
J-V Characteristics of the CdS/SnSe solar cell under different recombination mechanisms with representative and ideal resistance values.

Representative resistances				
Recombination	Voc (V)	Jsc (mA/cm^2)	Fill factor (%)	Efficiency (%)
R-IR-SRH	0.38	5.70	32	0.7
R–SRH	0.44	5.71	30	0.8
R–IR	0.49	16.32	26	2.1
R	0.69	21.68	28	4.3
Ideal resistances				
R-IR-SRH	0.42	7.57	58	1.8
R–SRH	0.51	7.57	57	2.2
R–IR	0.50	28.60	69	9.9
R	0.71	28.61	81	16.4
Experimental				
Shinde et al. [10]	0.37	5.73	30	0.63

obtained when the radiative recombination is the only loss mechanism in the device, with J_{sc} and V_{oc} around 22 mA/cm^2 and 0.7 V, respectively. Conversely, the poorest solar cell characteristics are exhibited when all recombination mechanisms are present. However, the most relevant result is that the SRH recombination is the main responsible for current and voltage losses in the solar cell. The lifetime of charge carriers inversely depends on the defect density in the bulk semiconductor, so the higher the density of defects the shorter the charge carrier lifetime, which is in good correspondence with previous results on other chalcogenides such as antimony sulfide selenide, in which shorter minority carrier lifetime values yielded lower efficiency and V_{oc} values [26]. Table 2 shows that defects at the CdS/SnSe interface have a lower impact on carrier transport than SnSe bulk defects, however, it should be noted that the interface recombination cannot be neglected since efficiency is limited to 2.1 % under this mechanism, demonstrating the important role of carrier recombination due to cliff-like band alignment. Under the radiative limit, only a 4.3 % efficiency is observed, which indicates the necessity of analyzing other factors such as resistances. Fig. 7(b) and Table 2 illustrate general solar cell improvement under ideal series and shunt resistances, showing that an important issue concerning this type of solar cell is the effect of resistances. In addition, beyond the optoelectronic parameter values, a similar trend is observed for the transport mechanisms under ideal resistances, in which bulk defects are dominant rather than interface defects. However, even under ideal resistances, if the CdS/SnSe interface recombination were dominant, efficiency would be limited to values lower than 10 %, making also this mechanism important in SnSe solar cells.

Buffer and absorber thickness variation on the J-V characteristics

To evaluate the impact of buffer and absorber thicknesses on the photovoltaic characteristics, both CdS and SnSe thicknesses were varied from 25 to 200 nm and 0.4 to 5 μm, respectively. For these calculations, the presence of representative resistances and ideal resistances is being considered. Defect densities of 1 x 10^{20} cm^{-3} and 8 x 10^{17} cm^{-3} were considered for SnSe and CdS materials, respectively, while at the CdS/SnSe interface, a concentration of 1.5 x 10^{7} cm^{-2} was taken into account. The primary motivation for varying the thickness of the layers that make up the junction is given by the remarkable relationship existing between the thickness and the optical absorption coefficient, diffusion length, and lifetime of the charge carriers, which affects the generation and recombination rates of solar cells. In general, a small thickness is desirable for the buffer region since most of the incident light will reach the absorber region without being absorbed by the buffer, in this way taking advantage of the short wavelengths of the ultraviolet region and avoiding the effect of parasitic absorptions [27,28]. On the other hand, the thickness of the absorber is typically the highest, but without exceeding both the length that light can travel into the absorber and the diffusion length of carriers for a better carrier collection, so there is an optimal thickness depending on the loss mechanisms governing the device. Beyond this optimal thickness, the charge carriers contributing to the photocurrent are not so significant. Fig. 8 shows SnSe solar cell characteristics for different CdS buffer thicknesses under representative resistances and the different recombination mechanisms. The solar cell behavior with the increment of buffer thickness varies according to the recombination mechanisms acting at the time. For the radiative with interface recombination mechanisms (R-IR), and radiative with Shockley-Read-Hall recombination (R-SRH), the open-circuit voltage has contrasting behavior for thicknesses lower than 84 nm (Fig. 8(a)). For R-IR, the V_{oc} decreases from 0.62 V to 0.50 V between 25 nm and 84 nm, and then it remains steady around 0.48 V for higher thicknesses. A higher CdS thickness results in higher parasitic absorption near the CdS/SnSe interface, thereby reducing V_{oc} to a value of 0.5 V, which is kept constant for CdS thicknesses higher than 84 nm since carriers photogeneration takes place away from the effect of interface defects. On the other hand, for the R-SRH mechanism, V_{oc} slightly increases to 0.45 V as the thickness enlarges, remaining unchanged at this value for thicknesses greater than 60 nm. This increment is due to a small amount of light being absorbed near the depletion region in the CdS material, instead of penetrating deeply into the absorber where the generated charge carriers recombine before they can reach the depletion region due to the presence of SnSe bulk defects. However, when the thickness of the buffer increases above 60 nm, the light absorbed in the buffer layer far from the depletion zone does not contribute to the charge collection due to the short diffusion length in CdS owing to the bulk recombination. The behavior of J_{sc} shown in Fig. 8

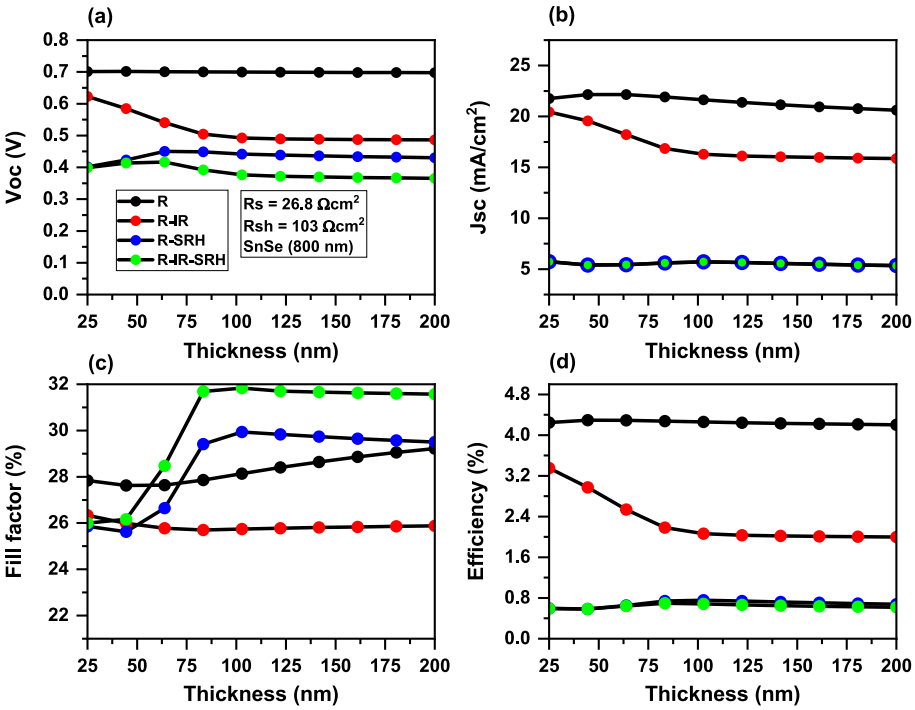

Fig. 8. The solar cell optoelectronic parameters for different buffer thicknesses and recombination mechanisms under representative resistances.

(b) is such that when there is no SRH recombination, Jsc values are above 15 mA/cm^2, and it decreases when the thickness increases owing to the buffer parasitic losses. However, absorber defects drastically reduce J_{sc} to values lower than 7 mA/cm^2. Fig. 8(b) illustrates that J_{sc} values are mostly dominated by the SnSe bulk defects. A general result is that short FF values are obtained for solar cells under all transport mechanisms as presented in Fig. 8(c). In addition, Fig. 8(d) demonstrates that efficiencies for R-IR-SRH and R-SRH under representative

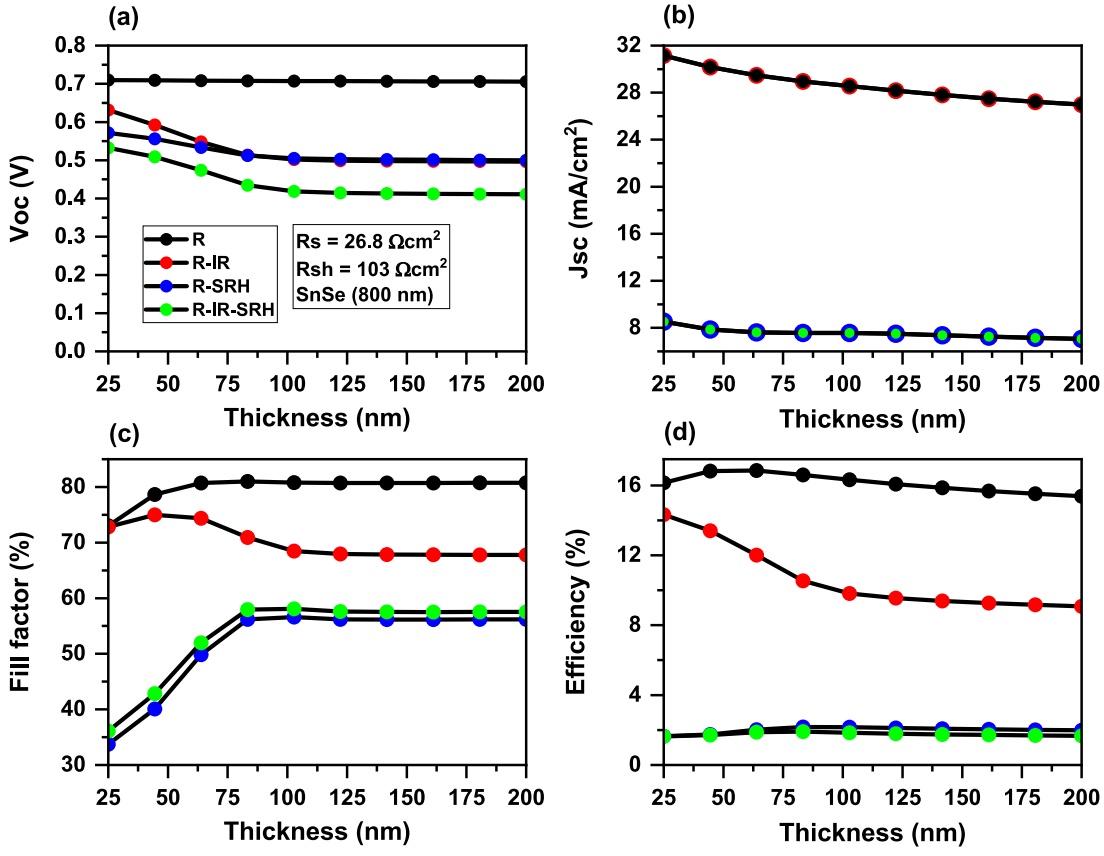

Fig. 9. The solar cell optoelectronic parameters for different buffer thicknesses and recombination mechanisms under ideal resistances.

resistances are quite similar and lower than 4.5 %, being their trend consistent with the behavior of V_{oc}, J_{sc}, and fill factor.

Fig. 9 presents the optoelectronic characteristics under ideal resistances for different buffer layer thicknesses. It is noticed that the fill factor under ideal resistances is greater than under representative resistances, this implies that better use of the received power is attained for small series and high shunt resistance values, which shows that one of the major issues with this kind of solar cells is the resistance values reported so far [6]. Under ideal resistances, it is possible to achieve higher V_{oc} and J_{sc} values, which along with a high fill factor, yield higher efficiencies. Under this regime, the main limiting factor concerns the charge carrier recombination, for R-SRH and R-IR-SRH the efficiency is limited in such a way that it is not affected by variations in the buffer thickness. Due to the high defect density in the absorber region, the diffusion length is too short that only charge carriers generated in the depletion region are collected, and there is an offset between the generation and recombination rates, which results in roughly the same efficiency for different buffer thicknesses. It is demonstrated that if the CdS/SnSe interface losses were dominant, efficiency values of about 10 % would be achieved in this technology. For the radiative recombination mechanism, the efficiency reaches the maximum value around a thickness of 50 nm, where high values of V_{oc}, J_{sc}, and FF are achieved as well. Thus, a thickness of 50 nm can be used as an optimal value for the next calculations.

In the next step, the influence of CdS donor concentration in the range of 10^{15} to 10^{18} cm^{-3} and thickness in the range of 20 to 150 nm on SnSe solar cells is evaluated and analyzed in detail, considering the simultaneous contribution of all loss mechanisms. The impact of CdS donor concentration and thickness on Voc under and without the presence of resistances is presented in Fig. 10. In general, a Voc variation from 0.25 to 0.42 V is observed under the presence of resistances, while Voc values ranging from 0.28 to 0.55 V are found for ideal resistances. For a CdS donor concentration lower than 10^{17} cm^{-3}, the increment of CdS thickness, and the reduction in CdS donor concentration contribute to a slight Voc decrease under the presence of resistances, while in the case of ideal resistances Voc is nearly independent of the CdS concentration and thickness. This result is mainly because of carrier recombination, which is more drastic under low CdS donor density and higher thickness under the effect of resistances. For the highest CdS donor densities, the impact of CdS thickness on Voc is nearly the same under and without resistances, due to the low impact of CdS thickness on carrier recombination. Fig. 10 also shows that a CdS donor concentration of about 10^{17} cm^{-3} and CdS thicknesses ranging from 20 to 70 nm result in the best Voc values. Conversely, the lowest CdS donor concentrations allow the highest Voc values in the absence of resistances. The Jsc dependence on CdS donor concentration and thickness is shown in Fig. 11. The highest Jsc values are obtained at the lowest CdS thicknesses and the biggest CdS donor concentrations for SnSe solar cells with and without resistances. A high CdS donor concentration allows the depletion layer to broaden at the SnSe absorber material, thereby guaranteeing a higher carrier separation and collection. In addition, since higher CdS thicknesses result in a lower transmittance due to the higher parasitic absorption at the CdS, the best Jsc values are obtained for the lowest CdS thicknesses, which is in good correspondence with other solar cell technologies where CdS has been used as the buffer layer [29]. The presence of typical resistance values is translated into a Jsc reduction of about 2.7 mA/cm^2 as shown in Fig. 11. The effect of CdS donor concentration and thickness variations under and without the effect of resistances on the fill factor is shown in Fig. 12. For CdS donor concentrations lower than 10^{17} cm^{-3}, modest changes are found. Conversely, CdS donor concentrations in the range of 10^{17}–10^{18} cm^{-3} favor carrier transport thereby reducing series resistances and resulting in higher fill factor values. Fig. 12 also shows a drastic drop in the maximum expected fill factor from 61 % to almost 32 % under the presence of resistances. This highlights the importance of reducing the effect of resistances in SnSe device promotion. The SnSe solar cell efficiency behavior as a function of CdS donor concentration and thickness is presented in Fig. 13. For CdS donor concentrations lower than 10^{17} cm^{-3}, similar trends are observed for devices with and without resistances, where the decrease in CdS donor concentration and the increase in CdS thickness result in the lowest SnSe solar cell efficiencies. This result is directly related to the Jsc behavior as presented in Fig. 11. On the other hand, CdS donor concentrations in the range of 10^{17}–10^{18} cm^{-3} and CdS thicknesses ranging from 50 to 100 nm allow maximum solar cell efficiencies. In particular, maximum efficiency values of 0.69 and 1.92 % can be achieved for SnSe solar cells with and without resistances, pointing out the need to focus on recombination losses rather than device resistances for solar cell efficiency promotion. Fig. 13 demonstrates that a CdS thickness of 50 nm can still be considered optimal in other calculations to avoid increased CdS parasitic losses.

To determine an appropriate absorber thickness, calculations are carried out for a fixed buffer thickness of 100 nm and absorber thicknesses ranging from 0.4 to 5 μm. The effect of both representative and ideal resistances for each recombination mechanism is taken into consideration. The first remarkable aspect to notice when inspecting both Fig. 14 and Fig. 15 is that the increment of thickness in the absorber leads to an increment in V_{oc}, J_{sc}, and as a consequence the efficiency when transport mechanisms such as radiative and interface recombination are dominant. In particular, a slight variation is observed under the IR mechanism, while when SRH is dominant, solar cell characteristics are nearly independent of thickness. This is a result of the high impact of bulk defects on carrier transport in this type of structure, preventing photogenerated carriers from reaching the depletion zone. A different trend is observed for the fill factor of the solar cell with

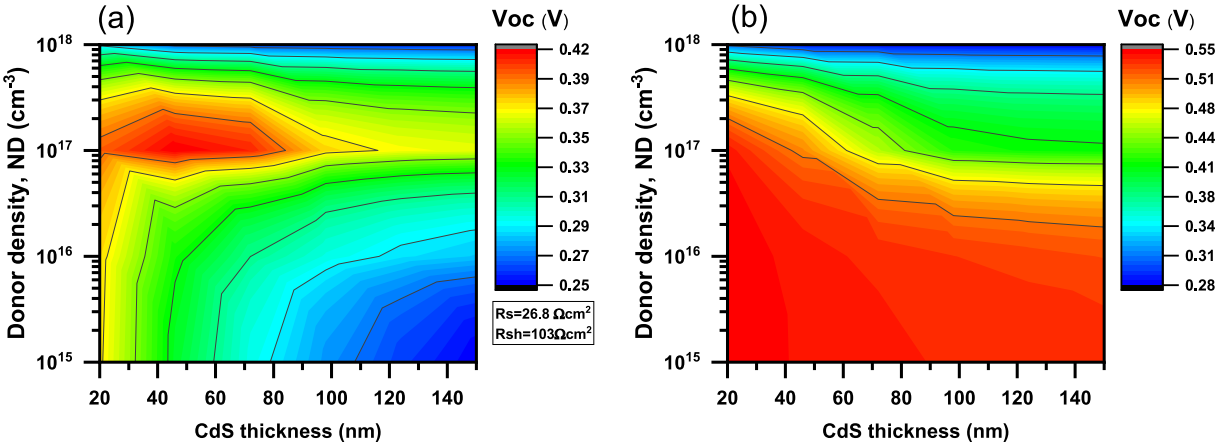

Fig. 10. V_{oc} for different CdS donor concentrations and thicknesses in SnSe solar cells. Under (a) representative resistances and (b) ideal resistances.

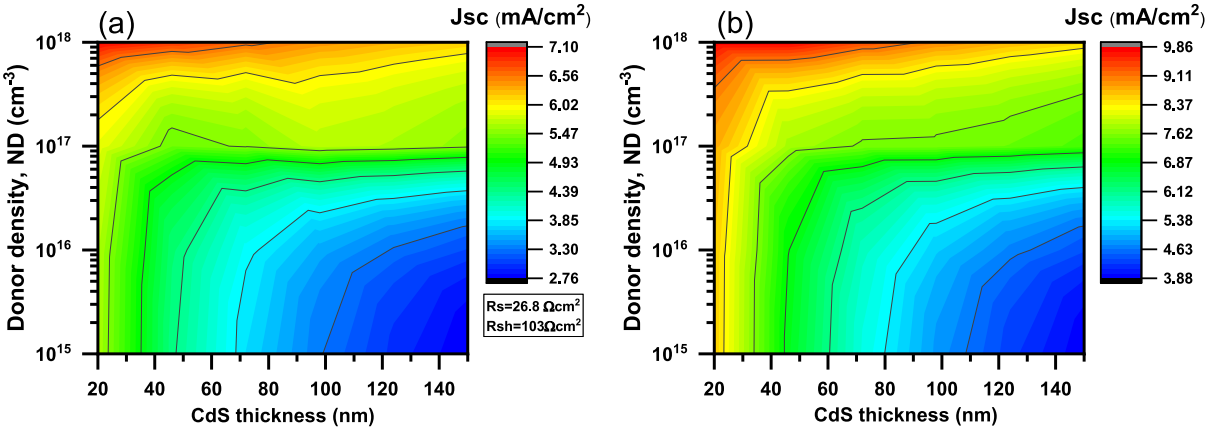

Fig. 11. Jsc for different CdS donor concentrations and thicknesses in SnSe solar cells. Under (a) representative resistances and (b) ideal resistances.

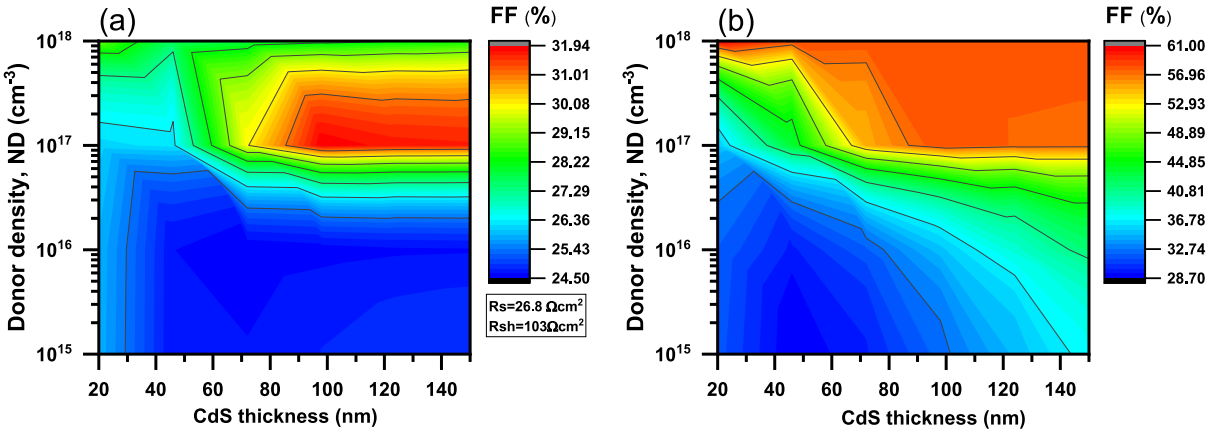

Fig. 12. FF for different CdS donor concentrations and thicknesses in SnSe solar cells. Under (a) representative resistances and (b) ideal resistances.

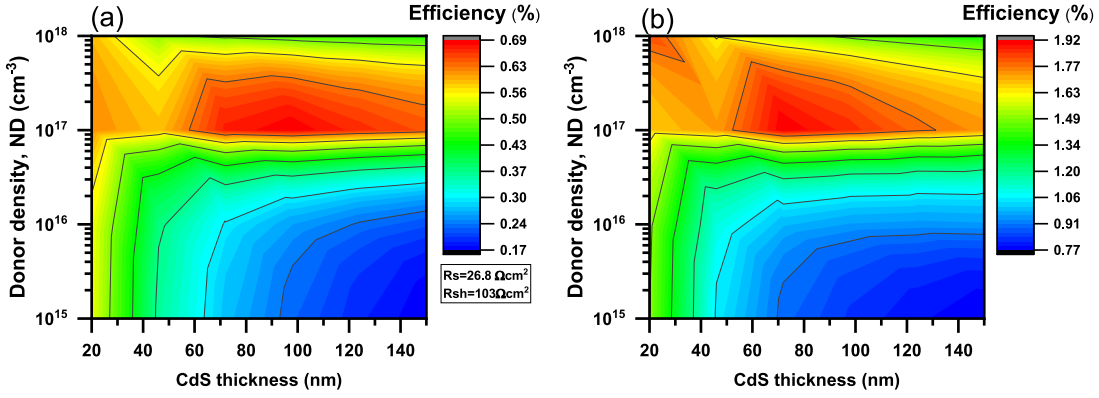

Fig. 13. Efficiency dependence on CdS donor concentration and thickness in SnSe solar cells. Under (a) representative resistances and (b) ideal resistances.

representative and ideal resistances. When representative resistances are assumed for calculations, the increment in thickness results in higher series resistances, thereby reducing Jsc and also the fill factor as observed under the R and R-IR mechanisms. However, under the effect of bulk defects that play the most important role in carrier losses, the fill factor is not affected by the variation of absorber thickness. A remarkable difference is also observed for Jsc under R and R-IR mechanisms. Under the presence of representative resistances, lower Jsc values for the R-IR mechanism are obtained but when resistances are neglected Jsc values corresponding to both R and R-IR mechanisms are nearly the same, which accounts for resistive losses at materials and semiconductor/metal contact rather than losses at CdS/SnSe interface. In general, Voc presents a very short variation with absorber thickness changes for all the transport mechanisms. Figs. 14 and 15 also demonstrate that the low efficiency reported for CdS/SnSe solar cells is mainly a result of very low Jsc values due to the effect of SnSe bulk defects along with losses due to resistances. The reduction of SnSe defects could by itself result in an efficiency promotion from 0.8 % to 2.2 %, being also necessary the mitigation of parasitic resistance effects to accomplish performance values of 10 %. For further calculations, a SnSe thickness of 1.7 μm is considered, for which efficiency values are near the maximum ones.

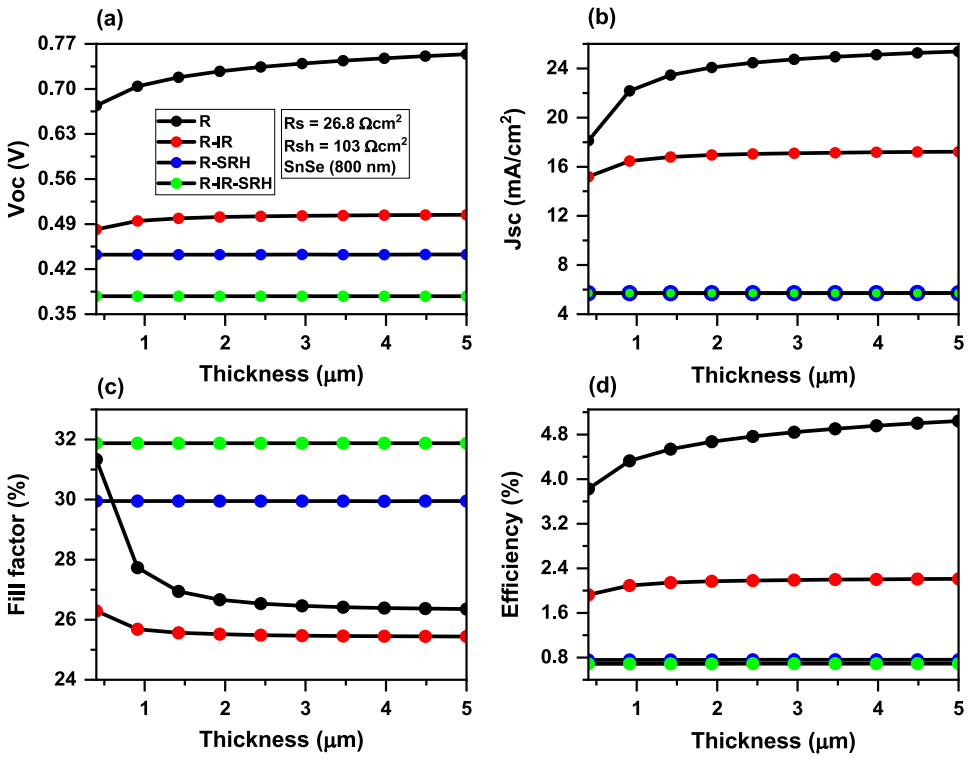

Fig. 14. The solar cell optoelectronic parameters for different absorber thicknesses and different recombination mechanisms under representative series and shunt resistances.

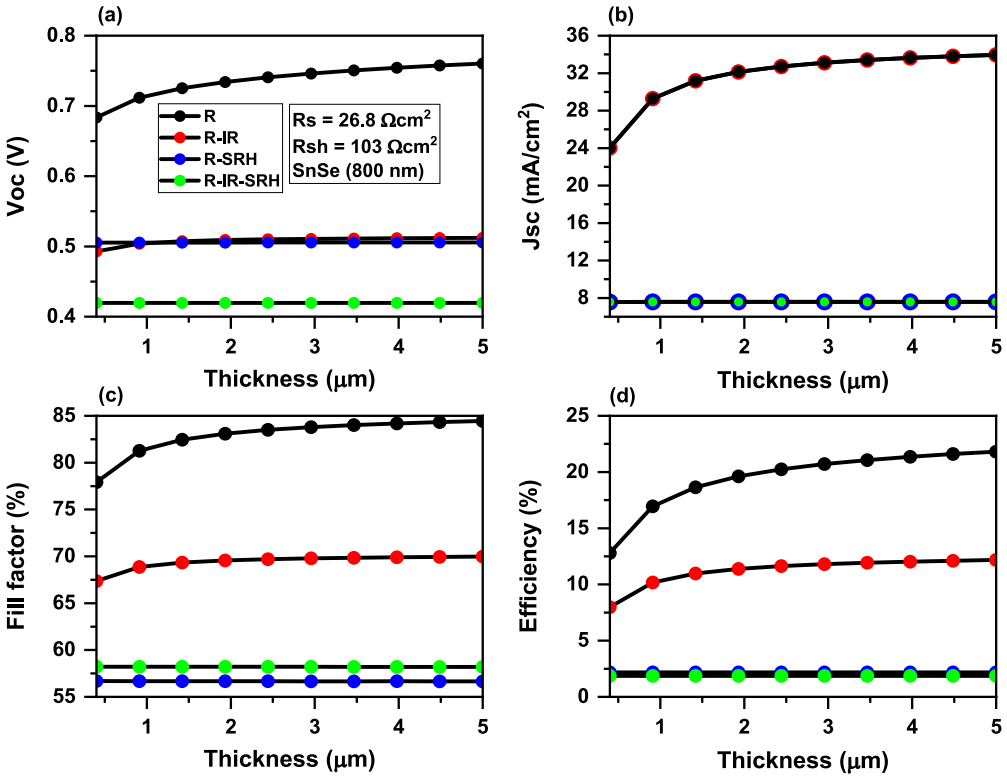

Fig. 15. The solar cell optoelectronic parameters for different absorber thicknesses and different recombination mechanisms under ideal resistances.

SnSe bulk defects vs surface defects at the CdS/SnSe interface

So far, SnSe bulk and CdS/SnSe interface defects have been demonstrated to be dominant under the effect of resistances. The knowledge of the influence of these defects on SnSe solar cells under and without the effect of resistances is required to promote this technology. The SnSe bulk and CdS/SnSe interface defect effect on Voc for SnSe solar cells under and without the effect of resistances is illustrated in Fig. 16.

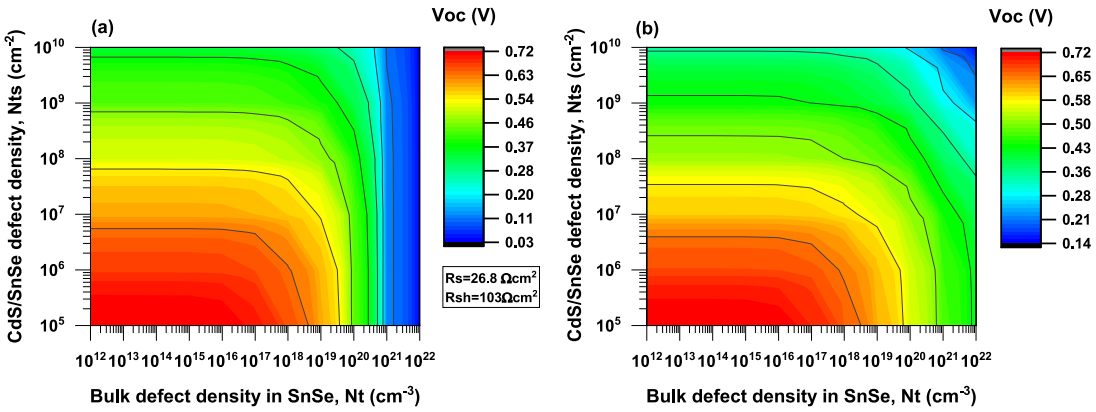

Fig. 16. V_{oc} for different surface defect densities at the CdS/SnSe interface and bulk defect densities in SnSe. Under (a) representative resistances and (b) ideal resistances. For calculations, SnSe and CdS thicknesses of 1.7 μm and 50 nm, respectively were considered.

In general, the best V_{oc} values are obtained when bulk defect density is low, being V_{oc} more sensitive to bulk defects than interface defects when interface defect density values are lower than 10^8 cm^{-2}. For higher interface defect concentration values, Voc is almost constant for SnSe bulk defects shorter than 10^{20} cm^{-3}, which indicates that CdS/SnSe interface losses become dominant. V_{oc} values close to 0.7 V are shown for CdS/SnSe and SnSe defect densities lower than 10^6 cm^{-2} and 10^{16} cm^{-3}, respectively. Fig. 16 also demonstrates that for SnSe bulk defect densities higher than 10^{21} cm^{-3} and under the effect of resistances, V_{oc} is independent of the CdS/SnSe interface defect density, while under the ideal resistances, an increment in Voc is expected with the reduction of CdS/SnSe interface defect density. However, a similar maximum V_{oc} of 0.72 V is expected for optimized devices with and without the effect of resistances, being only noticeable the effect of resistances in the region of SnSe bulk defect density higher than 10^{21} cm^{-3}. In general, since Voc is almost the same with and without the effect of resistances, we can elucidate that high series resistances are limiting the device performance.

Fig. 17 shows that resistances are an important issue in CdS/SnSe devices. Jsc values independent of defect density at the CdS/SnSe interface are obtained for a bulk defect density larger than 10^{19} cm^{-3}, which indicates that under a high bulk defect density the influence of interface defects is almost negligible. The increase of bulk defect density results in the Jsc reduction as expected since SRH recombination increases. Under the effect of representative resistances, Jsc values are shorter. On the other hand, when bulk defect density is shorter than 10^{19} cm^{-3}, an increase in Jsc is found with the reduction of CdS/SnSe interface and SnSe bulk defect densities even under the influence of resistances. However, in this regime, bulk defects have a more dominant role than interface defects. Fig. 17 also illustrates that in the device without resistances, the CdS/SnSe interface defects impact on Jsc is almost negligible. The negative effect of series resistances in CdS/SnSe solar cells is demonstrated by the Jsc drop from 33.3 to 23.9 mA/cm^2.

The influence of SnSe bulk and CdS/SnSe interface defects on efficiency is presented in Fig. 18 under the effect of representative resistances (a) and ideal resistances (b). Fig. 18(a) shows that the highest efficiency that can be attained is around 3 % considering the technical limitations to obtain the level of defects that would allow this; this value of efficiency is in correspondence with a reported work on CdS/SnSe solar cells [15]. Fig. 18(b) shows that under the negligible effect of resistances during the calculations, efficiencies ranging from 12 % to 19 % can be achieved considering the optimal thicknesses of SnSe and CdS, and N_t from 2 x 10^{16} to 1 x 10^{18} cm^{-3} along with N_{ts} from 7 x 10^5 to 2 x 10^8 cm^{-2}, respectively. The highest efficiencies can be obtained for bulk and interface defect density values lower than 10^{17} cm^{-3} and 10^6 cm^{-2}, respectively. Conversely, the lowest efficiency values are observed in both devices for bulk density values higher than 10^{20} cm^{-3}, for which the effect of interface defects can be almost neglected. This figure also demonstrates that under ideal resistances, the effect of interface defects would be more detrimental for the device when bulk defect density is lower than 10^{18} cm^{-3} since efficiency variations from 1.2 % to 4.5 % are found depending on interface defects under the effect of resistances, while a variation from 5 % to 19.4 % is expected for ideal resistances.

Acceptor concentration vs bulk defects in SnSe

In typical structures, the acceptor concentration in the p-type semiconductor influences the depletion width in the buffer region and therefore the strength of the electric field that will separate the electron-hole pairs and will contribute to increasing the photocurrent. To find the

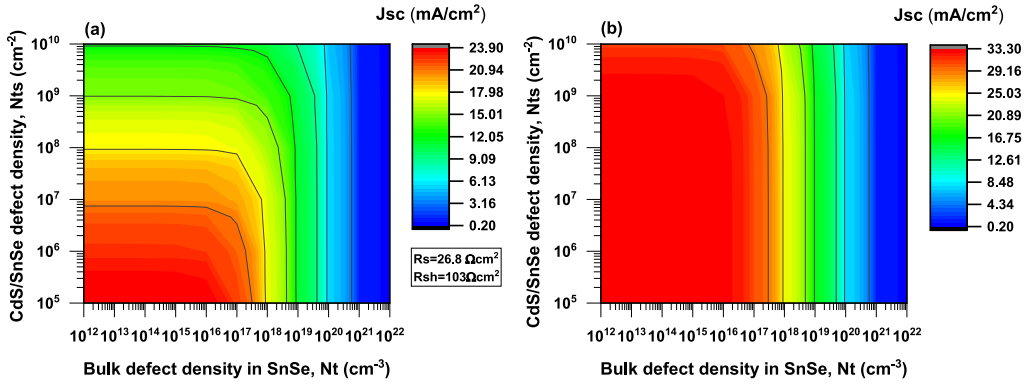

Fig. 17. J_{sc} for different surface defect densities at the CdS/SnSe interface and bulk defect densities in SnSe. Under (a) representative resistances and (b) ideal resistances. For calculations, SnSe and CdS thicknesses of 1.7 μm and 50 nm, respectively were considered.

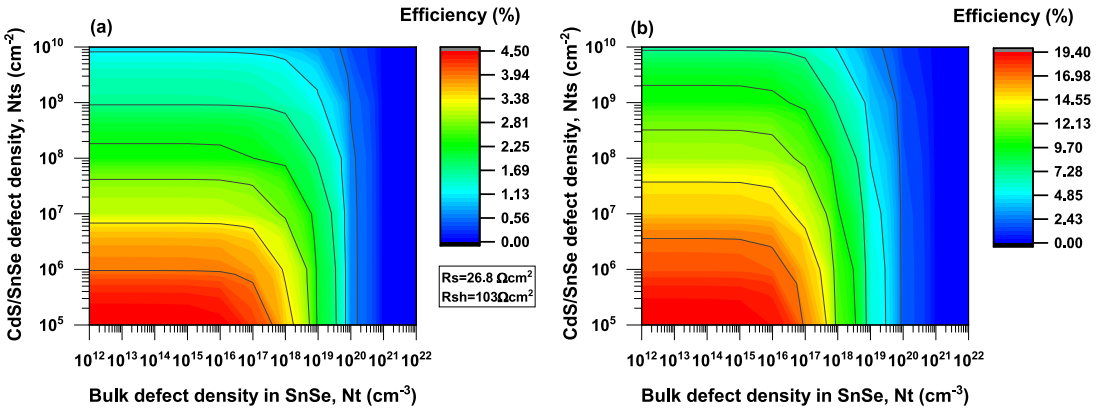

Fig. 18. Efficiency for different surface defect densities at the CdS/SnSe interface and bulk defect densities in SnSe. Under (a) representative resistances and (b) ideal resistances. For calculations, SnSe and CdS thicknesses of 1.7 μm and 50 nm, respectively were considered.

SnSe acceptor concentration value that optimizes the device performance, the variation of both acceptor concentration and bulk defect concentration was carried out. Results on the Voc, Jsc, and efficiency are given in Figs. 19, 20, and 21, respectively. For the calculations, the thickness of the absorber and buffer layers are 1.7 μm and 50 nm, respectively, and the CdS/SnSe interface defect density is 10^6 cm^{-2}. The increment of the acceptor density concentration in the absorber gets the quasi-fermi energy level of holes close to the valence band allowing higher V_{oc} values of around 0.85 V as seen in Fig. 19, whereas the bulk defect density does not affect the Voc as far as it is kept lower than 10^{17} cm^{-3}. In addition, series resistances in the device do not affect the V_{oc} values, and it is demonstrated that the low shunt resistance value has a negligible effect. Conversely, Jsc is drastically affected by the presence of resistance. In Fig. 20(a), the highest J_{sc} values are around 23 mA/cm^2 under representative resistances, however, under ideal resistances, these values can be around 33 mA/cm^2 for the same range of acceptor and defect concentrations as shown in Fig. 20(b). Consequently, series resistances are dominant in SnSe solar cells. For bulk defect concentrations lower than 10^{17} cm^{-3}, an increase in Jsc from about 13 to 25 mA/cm^2 is expected with increasing acceptor concentration as depicted in Fig. 20 (a), whereas under ideal resistances Jsc barely changes as shown in Fig. 20(b). Bulk defect concentrations lower than 10^{17} cm^{-3} have a negligible impact on Jsc values under representative and ideal resistances. Conversely, bulk defect concentrations higher than 10^{17} cm^{-3} would increase carrier losses, drastically reducing the carrier collection and thereby Jsc; under this regimen the effect of acceptor concentration is negligible. The increment in Jsc for higher acceptor concentrations is related to the increment in electron-hole pairs collection due to a stronger electric field. On the other hand, due to the slight variation of V_{oc} and Jsc for bulk defect density values lower than 10^{17} cm^{-3}, solar cell efficiency in this range is nearly constant for a particular acceptor density value as shown in Fig. 21(a) and (b). Besides, in such a range, the device shows a clear dependence of efficiency on acceptor concentration under representative and ideal resistances. Unlike the case of ideal resistances for which the increase of acceptor concentration would result in an efficiency increase from 13 % to 23 %, when representative resistances are considered in the calculations, efficiency is only increased from about 2 % to 6.3 %, which is still higher than the current highest efficiency achieved experimentally. Even though the solar cell efficiency increases, the resistances degrade the photovoltaic characteristics. This result is mainly due to the impact of resistances on Jsc, since Voc remains steady under representative and ideal resistances, thereby highlighting the need to reduce the effect of series resistances on Jsc for the next efficiency promotion. For the solar cell optimization, an acceptor density of 2 x 10^{19} cm^{-3} will be considered in the next calculations.

Temperature effect on SnSe solar cell

The temperature effect on SnSe solar cells is presented in Fig. 22, where temperatures ranging from 250 K to 400 K were evaluated. For calculations, experimental band gap values reported in the literature for SnSe were considered [30]. In particular, a linear decrease function of band gap with temperature was assumed as reported experimentally for SnSe material, accounting for $\beta = 0$ in the typical equation of semiconductor band gap variation with temperature, reported by Varshni [31]. By using Varshni's equation, it is possible to evaluate the SnSe band gap for temperatures in the range 250–400 K. Fig. 22(a) shows the J-V characteristics, while the behavior of the optoelectronic parameters

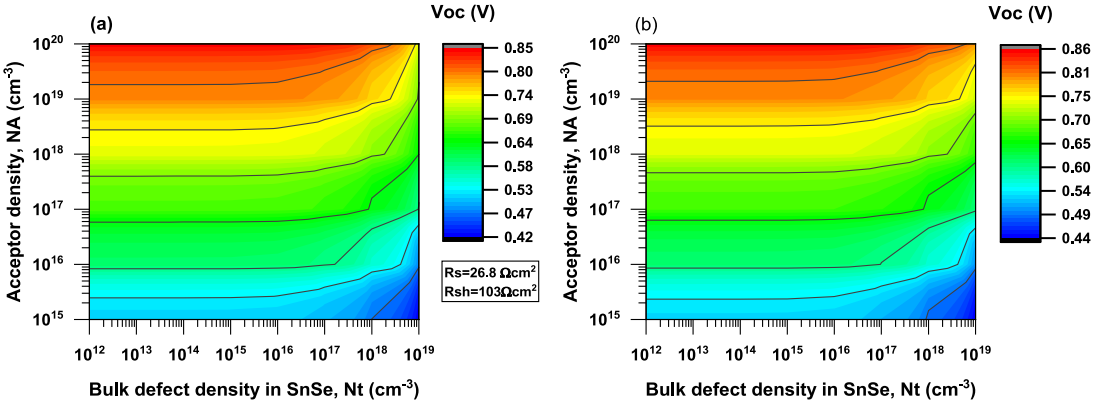

Fig. 19. V_{oc} for different acceptor densities and bulk defect densities in SnSe. Under (a) representative resistances and (b) ideal resistances. For calculations, an interface defect density of 10^6 cm^{-2} as well as SnSe and CdS thicknesses of 1.7 μm and 50 nm, respectively were considered.

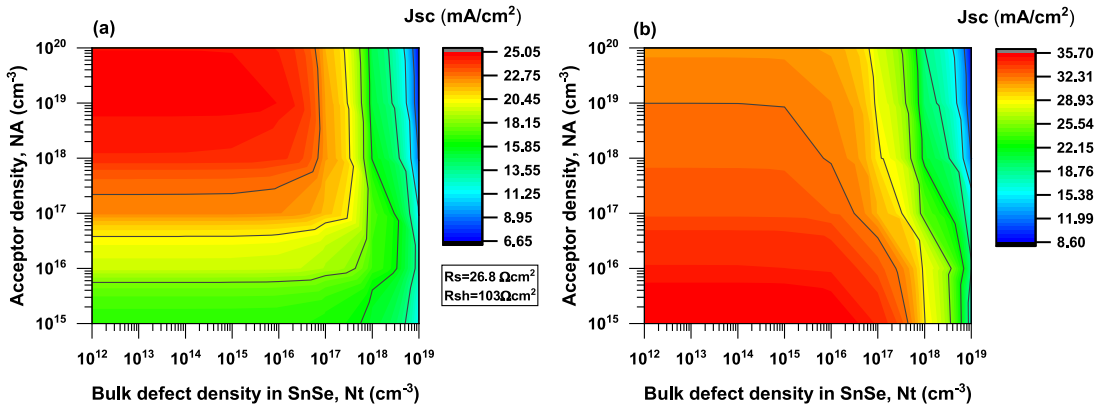

Fig. 20. J_{sc} for different acceptor densities and bulk defect densities in SnSe. Under (a) representative resistances and (b) ideal resistances. For calculations, an interface defect density of 10^6 cm^{-2} as well as SnSe and CdS thicknesses of 1.7 μm and 50 nm, respectively were considered.

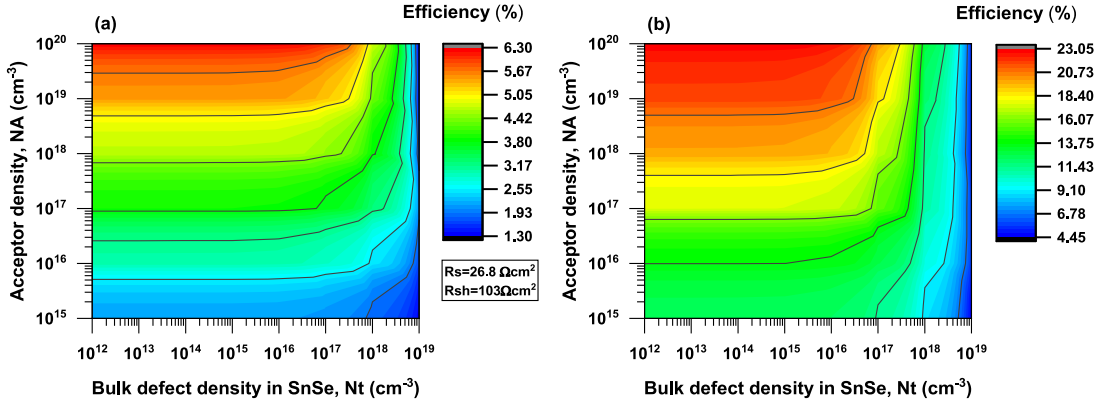

Fig. 21. Efficiency for different acceptor densities and bulk defect densities in SnSe under (a) representative, and (b) ideal resistances. For calculations, an interface defect density of 10^6 cm^{-2} as well as SnSe and CdS thicknesses of 1.7 μm and 50 nm, respectively were considered.

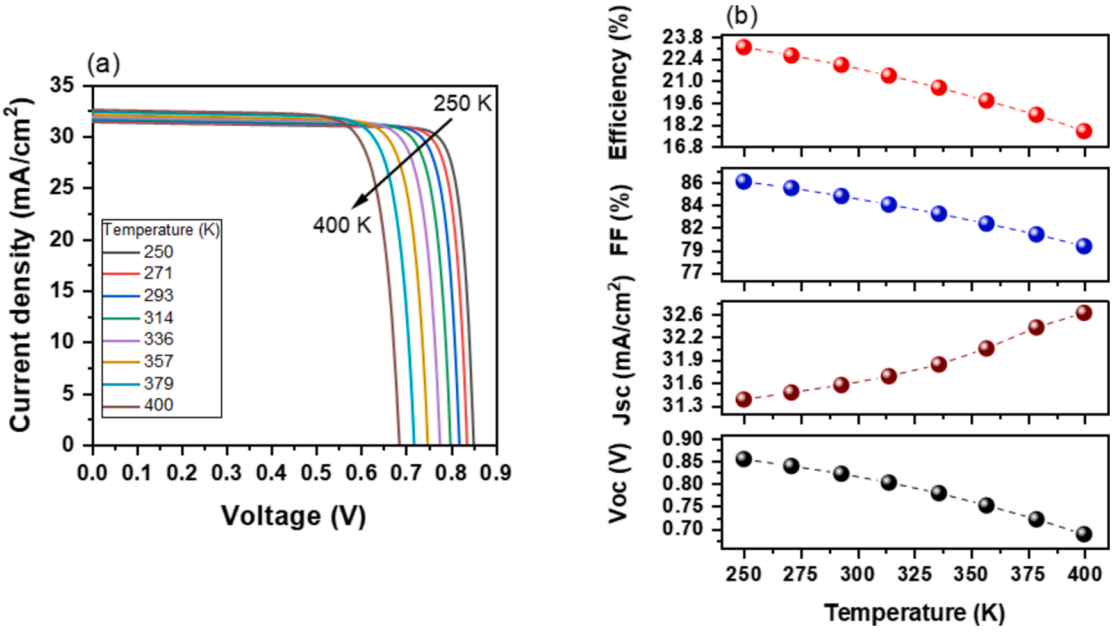

Fig. 22. Effect of temperature variation from 250 K to 400 K on (a) J-V characteristics and (b) optoelectronic parameters of SnSe solar cells under optimized conditions.

with the temperature is presented in Fig. 22(b). The temperature increase is translated into a Jsc increase and a Voc reduction, which is due to the band gap decrease with temperature. The band gap decrease favors higher photon absorption, thereby promoting Jsc of SnSe solar cell but Voc is reduced owing to the increased carrier recombination rate. Since higher temperatures contribute to bigger disorder in carrier transport, the fill factor is decreased. These parameters contribute to an efficiency degradation from 23.1 % to 17.8 % with the temperature increasing from 250 K to 400 K.

Photovoltaic characteristics of the optimized vs non-optimized devices

The J-V curves of both optimized and non-optimized solar cells have been calculated for comparison. The final optimal parameters and those first used to reproduce the experimental data given by Shinde et al are given in Table 3. Fig. 23 shows the comparison of both J-V results, where it is observed that the optimized solar cell has a high FF since ideal resistances are being considered. The Jsc is 31.6 mA/cm^2, which is roughly 81 % of the maximum theoretical value established by the Shockley-Queisser limit, and around six times the value reported for the non-optimized solar cell [14]. As a result of the optimization of the acceptor density and defect densities, the open-circuit voltage also showed a significant increment to 0.82 V. Finally, an optimized CdS/SnSe solar cell efficiency of up to 22 % is expected, because of the high FF, Jsc, and Voc, demonstrating that SnSe is quite attractive for solar cell fabrication; nevertheless, further experimental studies are pending. Table 4 presents similar theoretical results reported for SnSe solar cells calculated under AM1.5G, room temperature, and ideal resistances. Voc, Jsc, FF, and efficiency values in the range of 467–890 mV, 28.48–38.62 mA/cm^2, 68.1–86.6 %, and 9.05–29.3 %, respectively have been theoretically reported for optimized SnSe solar cells, which are in good correspondence with the values reported in this work. Unlike some of the results reported in Table 4, our work demonstrates that it is possible to obtain optimized SnSe solar cell efficiencies higher than 20 % without the incorporation of a hole transport layer.

In order to achieve SnSe solar cell efficiencies higher than 20 % as expected under optimal conditions, several aspects should be addressed in laboratories. The main experimental challenges that the scientific community faces for fabricating highly efficient SnSe solar cells are the reduction of defects at SnSe bulk and CdS/SnSe interface, as well as the minimization of resistance impact. In previous review works, these points have been highlighted as important [6,38]. Aspects such as SnSe poor crystallinity, the formation of defects, small grain size, and the formation of secondary phases reduce diffusion length and consequently carrier collection, resulting in low Jsc values [6,38]. Despite CdS being commonly used as a buffer material in SnSe solar cells, its relatively low band gap contributes to parasitic absorption losses in the short wavelength region, and it is also characterized by the formation of a cliff-like band alignment, having a negative impact on the device performance. On the other hand, important disagreements in crystallographic structure and lattice parameters between SnSe and CdS result in the formation of interface defects, thereby enabling carrier recombination. In this sense, the fabrication of smooth surfaces, very thin passivation interfacial layers, or even the use of an alternative buffer layer with better band alignment and lattice matching to the SnSe film are important points for promoting SnSe solar cell performance. On the other hand, compact, smooth, and pin-hole-free layers can prevent leakage current, thereby increasing shunt resistance. The experimental study on SnSe doping to increase carrier concentration as well as the use of the alternative back contact with high work function resulting in ohmic contact at the SnSe/metal interface are also necessary to reduce the series resistance. The use of a thin anti-reflection coating (ARC) – with a thickness of one-quarter the wavelength of the incoming wave for which reflection reduction is desired to take advantage of interference – is also an attractive proposal to increase the Jsc of SnSe solar cells by reducing the reflection losses. The proper application of the quarter-wavelength ARC can improve the SnSe solar cell efficiency. In general, secondary phase formation, bulk and interface defects, band alignment, absorber doping, back contact, and the use of an ARC layer are currently opportunity areas for improving SnSe solar cells. All these points constitute a guide for experimental groups working on SnSe solar cells for the further promotion of this technology.

Table 3
Parameters of the optimized solar cell and the non-optimized solar cell.

Parameters	Shinde et al. (SCAPS)	Optimized solar cell.
T_{CdS}, t_{SnSe}	100 nm, 800 nm	50 nm, 1.7 μm
R_s, R_{sh}	26.8 Ω cm^2, 103 Ωcm^2	0, very high
N_{ts}	1.5 x 10^7 cm^{-2}	1 x 10^6 cm^{-2}
N_t	1 x 10^{20} cm^{-3}	1 x 10^{16} cm^{-3}
N_A	1 x 10^{17} cm^{-3}	2 x 10^{19} cm^{-3}

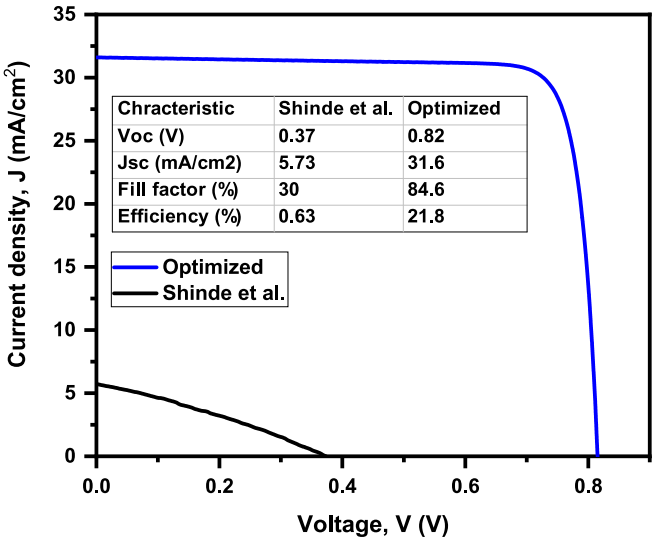

Fig. 23. Optimized vs non-optimized SnSe solar cell.

Table 4
Simulated photovoltaic characteristics of solar cells with SnSe absorber. All the simulations were performed under AM 1.5 solar spectrum, 300 K, and ideal resistances.

Structure	Voc (mV)	Jsc (mA/cm^2)	FF (%)	η (%)	Reference
ITO/CdS/SnSe/Ni	788	38.62	85.8	26.1	[32]
AZO/i-ZnO/CdS/SnSe/Mo	818	33.36	82.3	22.69	[15]
ITO/ZnO/Zn(O,S):N/SnO_2/SnSe/Mo	467	28.48	68.1	9.05	[33]
FTO/CdS/SnSe/CuI/Ni	860	32.99	86.2	24.5	[34]
FTO/CdS/SnSe/Sb_2Se_3/Au	840	38.42	86.6	28.2	[35]
FTO/WS_2/SnSe/Cu_2O/Ni	890	38.23	86.3	29.3	[36]
ZnO:Al/ZnO/ZnMgO/SnSe/NiO/Mo	823	33.45	74.8	20.59	[37]
ITO/CdS/SnSe/Au	820	31.60	85	21.8	This work

Conclusion

In summary, a numerical simulation was presented, where the impact of loss mechanisms such as radiative, SnSe bulk, and CdS/SnSe interface recombination was evaluated under and without the effect of resistances for the first time to get a better understanding of SnSe solar cell performance. The comparison between the model outcomes and the

experimental data showed good agreement, validating the important role of SnSe bulk defects and resistances in carrier losses. Furthermore, CdS/SnSe interface recombination was introduced as the second most important loss mechanism. We demonstrated that the simultaneous effect of radiative, SnSe bulk, and CdS/SnSe interface recombination can result in efficiencies of 0.7 % under the effect of resistances, while for ideal resistances efficiencies of about 1.8 % are expected. When the impact of the loss mechanisms is individually evaluated, efficiency values of 0.8 %, 2.1 %, and 4.3 % with resistances and 2.2 %, 9.9 %, and 16.4 % without resistances are obtained for SnSe bulk defect recombination, CdS/SnSe interface recombination, and radiative recombination, respectively. As a result, the first issues that must be addressed at laboratories are the reduction of both SnSe bulk defect density and resistance effect. However, it was pointed out that even under the negligible effect of SnSe bulk defects and resistances, SnSe solar cell efficiency would be limited to a value of 9.9 %, thereby requiring further studies to improve the CdS/SnSe interface. The detailed study on the effect of each loss mechanism on SnSe solar cells showed that an optimized solar cell efficiency of 21.8 % with Jsc, Voc, and FF values of 31.6 mA/cm^2, 0.82 V, and 84.6 %, respectively can be obtained by choosing N_A, N_t, and N_{ts} of 2 x 10^{19} cm^{-3}, 10^{16} cm^{-3}, and 10^6 cm^{-2} respectively, and with CdS and SnSe thicknesses of 50 nm and 1.7 μm, respectively, under ideal series and shunt resistances. In this sense, this work offers the route to further experimental improvement that would make this technology competitive with the current CdTe and CIGS ones.

CRediT authorship contribution statement

A. Carrillo-Osuna: Writing – original draft, Software, Methodology, Investigation, Formal analysis. **F.J. Sánchez-Rodríguez:** Writing – original draft, Validation, Software, Methodology, Investigation, Formal analysis, Data curation, Conceptualization. **K.G. Rodriguez-Osorio:** Writing – original draft, Validation, Software, Methodology, Investigation, Formal analysis, Data curation. **I. Montoya De Los Santos:** Writing – original draft, Validation, Software, Methodology, Investigation, Formal analysis, Data curation. **J.P. Morán-Lázaro:** Writing – original draft, Validation, Formal analysis, Data curation. **M. Ojeda-Martínez:** Writing – original draft, Validation, Formal analysis, Data curation. **Laura M. Pérez:** Writing – original draft, Validation, Methodology, Investigation, Funding acquisition, Formal analysis, Data curation. **David Laroze:** Writing – original draft, Validation, Methodology, Investigation, Funding acquisition, Formal analysis, Data curation. **Maykel Courel:** Writing – original draft, Visualization, Validation, Supervision, Resources, Project administration, Methodology, Funding acquisition, Formal analysis, Data curation, Conceptualization.

Declaration of competing interest

The authors declare that they have no known competing financial interests or personal relationships that could have appeared to influence the work reported in this paper.

Acknowledgment

The authors thank Marc Burgelman of Ghent University, Belgium, for generously providing the SCAPS program. Carrillo-Osuna thanks the financial support received by Conahcyt for master's degree studies. This work was partially supported by the project Fomento a la Investigación 2022 from the Universidad de Guadalajara. M. Courel thanks pro-SNI of Universidad de Guadalajara for the financial support. L.M.P. acknowledges financial support from the ANID through Convocatoria Nacional Subvención a Instalación en la Academia Convocatoria Año 2021, Grant SA77210040. LMP and DL acknowledge partial financial support from FONDECYT 1240985.

Data availability

Data will be made available on request.

References

[1] Green MA, Dunlop ED, Yoshita M, Kopidakis N, Bothe K, Siefer G, et al. Solar cell efficiency tables (version 63). Prog Photovoltaics Res Appl 2024;32(1):3–13. https://doi.org/10.1002/pip.3371.
[2] Le Donne A, Trifiletti V, Binetti S. New earth-abundant thin film solar cells based on chalcogenides. Front Chem 2019;7. https://doi.org/10.3389/fchem.2019.00297.
[3] Tao CS, Jiang J, Tao M. Natural resource limitations to terawatt-scale solar cells. Sol Energy Mater Sol Cells 2011;95:3176–80. https://doi.org/10.1016/j.solmat.2011.06.013.
[4] Huang Y, Wang C, Chen X, Zhou D, Du J, Wang S, et al. First-principles study on intrinsic defects of SnSe. RSC Adv 2017;7:27612–8. https://doi.org/10.1039/c7ra03367b.
[5] Kumar M, Rani S, Singh Y, Gour KS, Singh VN. Tin-selenide as a futuristic material: properties and applications. RSC Adv 2021;11:6477–503. https://doi.org/10.1039/d0ra09807h.
[6] Minnam Reddy VR, Gedi S, Pejjai B, Park C. Perspectives on SnSe-based thin film solar cells: a comprehensive review. J Mater Sci Mater Electron 2016;27:5491–508. https://doi.org/10.1007/s10854-016-4563-9.
[7] Shi W, Gao M, Wei J, Gao J, Fan C, Ashalley E, et al. Tin selenide (SnSe): growth, properties, and applications. Adv Sci 2018;5. https://doi.org/10.1002/advs.201700602.
[8] Vigil-Galán O, Espíndola-Rodríguez M, Courel M, Fontané X, Sylla D, Izquierdo-Roca V, et al. Secondary phases dependence on composition ratio in sprayed Cu_2ZnSnS_4 thin films and its impact on the high power conversion efficiency. Sol Energy Mater Sol Cells 2013;117:246–50. https://doi.org/10.1016/j.solmat.2013.06.008.
[9] Mathews NR. Electrodeposited tin selenide thin films for photovoltaic applications. Sol Energy 2012;86:1010–6. https://doi.org/10.1016/j.solener.2011.06.012.
[10] Shinde DV, Min SK, Sung MM, Shrestha NK, Mane RS, Han SH. Photovoltaic properties of nanocrystalline SnSe-CdS. Mater Lett 2014;115:244–7. https://doi.org/10.1016/j.matlet.2013.10.073.
[11] Abd El-Rahman KF, Darwish AAA, El-Shazly EAA. Electrical and photovoltaic properties of SnSe/Si heterojunction. Mater Sci Semicond Process 2014;25:123–9. https://doi.org/10.1016/j.mssp.2013.10.003.
[12] Barrios-Salgado E, Nair MTS, Nair PK. Chemically deposited SnSe thin films: thermal stability and solar cell application. ECS J Solid State Sci Technol 2014;3:Q169–75. https://doi.org/10.1149/2.0131408jss.
[13] Li Z, Guo Y, Zhao F, Nie C, Li H, Shi J, et al. Effect of film thickness and evaporation rate on co-evaporated SnSe thin films for photovoltaic applications. RSC Adv 2020;10:16749–55. https://doi.org/10.1039/D0RA01749C.
[14] Rühle S. Tabulated values of the Shockley-Queisser limit for single junction solar cells. Sol Energy 2016;130:139–47. https://doi.org/10.1016/j.solener.2016.02.015.
[15] Yadav RK, Pawar PS, Nandi R, Neerugatti KE, Kim YT, Cho JY, et al. A qualitative study of SnSe thin film solar cells using SCAPS 1D and comparison with experimental results: a pathway towards 22.69% efficiency. Sol Energy Mater Sol Cells 2022;244:111835. https://doi.org/10.1016/j.solmat.2022.111835.
[16] Kumar M, Rani S, Singh Y, Mamta A, Kumar VNS. Strategy to improve the efficiency of tin selenide based solar cell: a path from 1.02 to 27.72%. Sol Energy 2022;232:146–53. https://doi.org/10.1016/j.solener.2021.12.069.
[17] Gummel HK. A self-consistent iterative scheme for one-dimensional steady state transistor calculations. IEEE Trans Electron Devices 1964;11:455–65. https://doi.org/10.1109/T-ED.1964.15364.
[18] Im HS, Myung Y, Cho YJ, Kim CH, Kim HS, Back SH, et al. Facile phase and composition tuned synthesis of tin chalcogenide nanocrystals. RSC Adv 2013;3:10349. https://doi.org/10.1039/c3ra40869h.
[19] Sąfak H, Merdan M, Yüksel ÖF. Dispersion analysis of SnS and SnSe. Turkish J Phys 2002;26:341–7. https://journals.tubitak.gov.tr/physics/vol26/iss5/2.
[20] Ho CH, Lin WY, Chao LC, Lee KY, Inagaki J, Hsueh HC. Study of structural, thermoelectric, and photoelectric properties of layered tin monochalcogenides SnX (X = S, Se) for energy application. ACS Appl Energy Mater 2020;3:4896–905. https://doi.org/10.1021/acsaem.0c00481.
[21] Gray JL. "The Physics of the Solar Cell," in Handbook of Photovoltaic Science and Engineering, Chichester, UK: John Wiley & Sons, Ltd, 2011, pp. 82–129.
[22] Niemegeers A, Burgelman M, De Vos A. On the CdS/$CuInSe_2$ conduction band discontinuity. Appl Phys Lett 1995;67:843–5. https://doi.org/10.1063/1.115523.
[23] Hall RN. Electron-hole recombination in germanium. Phys Rev 1952;87:387. https://doi.org/10.1103/PhysRev.87.387.
[24] Shockley W, Read WTT. Statistics of the recombinations of holes and electrons. Phys Rev 1952;87:835–42. https://doi.org/10.1103/PhysRev.87.835.
[25] Pauwels HJ, Vanhoutte G. The influence of interface state and energy barriers on the efficiency of heterojunction solar cells. J Phys D Appl Phys 1978;11:649–67. https://doi.org/10.1088/0022-3727/11/5/009.
[26] Courel M, Jimenez T, Montoya De Los Santos I, Morán-Lázaro JP, Ojeda Martinez M, Pérez LM, Laroze D, Feddi E, Sánchez-Rodríguez FJ. Impact of loss mechanisms through defects on Sb2(S1-xSex)3/CdS solar cells with p-n structure. Eur Phys J plus 2022;137:396. https://doi.org/10.1140/epjp/s13360-022-02606-w.

[27] Powalla M, Paetel S, Ahlswede E, Wuerz R, Wessendorf CD, Magorian Friedlmeier T. Thin-film solar cells exceeding 22% solar cell efficiency: an overview on CdTe-, Cu(In,Ga)Se2 -, and perovskite-based materials. Appl Phys Rev 2018;5:041602. https://doi.org/10.1063/1.5061809.

[28] Cho JY, Kim S, Nandi R, Jang J, Yun H-S, Enkhbayar E, et al. Achieving over 4% efficiency for SnS/CdS thin-film solar cells by improving the heterojunction interface quality. J Mater Chem A 2020;8:20658–65. https://doi.org/10.1039/D0TA06937J.

[29] Moon MMA, Rahman MF, Kamruzzaman M, Hossain J, Ismail ABM. Unveiling the prospect of a novel chemical route for synthesizing solution-processed CdS/CdTe thin-film solar cells. Energy Rep 2021;7:1742–56. https://doi.org/10.1016/j.egyr.2021.03.031.

[30] Delice S, Isik M, Gullu HH, Terlemezoglu M, Bayrakli Surucu O, Parlak M, et al. Temperature dependence of band gaps in sputtered SnSe thin films. J Phys Chem Solids 2019;131:22–6. https://doi.org/10.1016/j.jpcs.2019.03.004.

[31] Varshni YP. Temperature dependence of the energy gap in semiconductors. Physica 1967;34:154. https://doi.org/10.1016/0031-8914(67)90062-6.

[32] Bhowmik A, Abir AT, Pappu MAH, Das SC, Mondal BK, Hossain J. Modeling and efficiency enhancement of SnSe thin film solar cell with a thin CIS layer. Results Mater 2023;21:100521. https://doi.org/10.1016/j.rinma.2023.100521.

[33] Montoya De Los Santos I, Cortina-Marrero HJ, Hechavarríía-Difur L, Sánchez-Rodríguez FJ, Meza-Avendaño CA, Borrego-Pérez JA, Moreno-Oliva VI, Román-Hernández E, Courel M. The effect of Se/(S+Se) compositional ratios on the performance of SnS-based solar cell: a numerical simulation. Semicond Sci Technol 2020;35. https://doi.org/10.1088/1361-6641/abadba.

[34] Khan TM, Khatun MM, Khatun H, Hosen A, Al Ahmed SR. "Design and Simulation of a Highly Efficient SnSe Solar Cell with CuI as an HTL by SCAPS-1D," *5th IEEE Int. Conf. Telecommun. Photonics, ICTP 2023 - e-Proceedings*, pp. 1–5, 2023, doi: 10.1109/ICTP60248.2023.10490748.

[35] Sultana B, Rahman MM, Harun-Or-Rashid M, Haque MD, Irfan A, Chaudhry AR, et al. A new design and optimization of SnSe-based dual absorber solar cell with efficiency above 28%. J Nanoparticle Res 2024;26:1–15. https://doi.org/10.1007/s11051-024-06085-1.

[36] Khan TM, Islam B, Ahmed SRA. Performance analysis and optimization of SnSe thin-film solar cell with Cu_2O HTL through a combination of SCAPS-1D and machine learning approaches. Mater Today Commun 2024;41:110490. https://doi.org/10.1016/j.mtcomm.2024.110490.

[37] Khadir A. Boosting the performance of SnSe-based solar cells through electron and hole transport layers: a qualitative study and perspectives. J Phys Chem Solid 2025;196:112333. https://doi.org/10.1016/j.jpcs.2024.112333.

[38] Beltrán-Bobadilla P, Carrillo-Osuna A, Rodriguez-Valverde JA, Acevedo-Juárez B, De Los Santos IM, Sánchez-Rodriguez FJ, Courel M. SnSe solar cells: current results and perspectives. Gen Chem 2021;7:200012. https://doi.org/10.21127/yaoyigc20200012.